Supporting information

Atomically Ordered PtM Intermetallics on Nitrogen-Doped Carbon for High-Efficiency Bifunctional Electrocatalysis

Yang Han[a], Qingmei Wang[a]*, Fengqin Zhang[a], Qingsong Hua[b]*, Shun Lu[c]*

a Guizhou University Key Laboratory of Green Chemical and Clean Energy Technology, Guizhou University Engineering Research Center of Efficient Utilization for Industrial Waste, School of Chemistry and Chemical Engineering, Guizhou University, Institute of Dual-carbon and New Energy Technology Innovation and Development of Guizhou Province, Guiyang, Guizhou, 550025, China.

b School of Physics and Astronomy, Beijing Normal University, Beijing 100875, China

c Chongqing Institute of Green and Intelligent Technology, Chinese Academy of Sciences, Chongqing 400714, China

* Corresponding authors:

qmwang3@gzu.edu.cn (Q. Wang); q.hua@bnu.edu.cn (Q. Hua);
lushun@cigit.ac.cn (S. Lu)

Contents

Experiment section

Soak 20 g of anion exchange resin in an ethanol solution (approximately 15 mL) for 10 hours. Subsequently, wash the resin cyclically three times with 10 wt% hydrochloric acid (HCl), deionized water, 10 wt% sodium hydroxide (NaOH), and deionized water. Ensure thorough rinsing with a large volume of deionized water during the final wash. Dry the resin afterward. Take 100 mg of treated Anion exchange resin, 2.5 mL of H_2PtCl_6, 50 mg of $K_3Co(CN)_6$ (50 mg of $K_3Fe(CN)_6$ or 37 mg of $K_2Ni(CN)_4$). Disperse these materials in 2.5 mL of ultra-pure water and stir at room temperature for 12 hours. After stirring, collect the PtM precursor and place it in a petri dish to dry naturally at room temperature. Heat the sample from 20 °C to 900 °C at a rate of 5 °C/min under a gas atmosphere consisting of 5% hydrogen (H_2) and 95% nitrogen (N_2). Maintain the temperature at 900 °C for 2 hours to complete the pyrolysis process. Grind the resulting material into a fine powder after the reduction and pyrolysis are completed. Wash the pyrolyzed sample with 2 mL of 30 wt% hydrogen peroxide (H_2O_2) at room temperature for 24 hours to remove impurities. Centrifuge the sample at 8500 rpm and wash it three times with ultra-pure water. Dry the sample afterward to obtain the PtM alloy catalyst (where M = Fe, Co, Ni).

Cyclic voltammetry (CV) was measured in N_2-saturated 0.1 M $HClO_4$ from 0.05 to 1.2 V vs RHE at 50 mV s^{-1}. ORR activity was measured by linear sweep voltammetry (LSV) at 1600 rpm in O_2-saturated 0.1 M $HClO_4$ at 5 mV s^{-1}. The electron transfer number (n) was calculated using the Koutecký–Levich (K-L) equation from ORR polarization curves recorded at rotation rates from 400 to 2500 rpm. The electrochemically active surface area (ECSA) was determined from CO stripping experiments. The electrode was saturated with CO in 0.1 M $HClO_4$ for 20 min, followed by a 30 min N_2 purge to remove dissolved CO before recording the stripping voltammogram. The accelerated durability test (ADT) for ORR was performed by cycling the potential between 0.6 and 1.2 V for 20,000 cycles in O_2-saturated 0.1 M $HClO_4$. MOR activity was measured in N_2-saturated 0.1 M $HClO_4$ containing 0.5 M methanol. Chronoamperometry (CA) was recorded at a constant potential of 0.75 V for 2000 s. The ADT for MOR involved 600 cycles at 0.75 V. ECSA and n were calculated as follows (**Equation 1**):

$$ECSA_{CO}=Q_{CO}/(0.42* [Pt]) \quad (1)$$

Q_{CO} represents the electric charge derived from the integration of the CO stripping voltammogram, while [Pt] denotes the platinum loading on the electrode surface, expressed in mg cm^{-2}

The electron transfer number (n) was determined through analysis of the ORR polarization curves acquired at rotation rates ranging from 400 to 2500 rpm, based on the first-order K-L equation (**Equation 2**):

$$\frac{1}{j} = \frac{1}{j_K} + \frac{1}{j_L} = \frac{1}{j_L} + \frac{1}{B\omega^{1/2}} \quad (2)$$

The measured current density (j) comprises both diffusion-limiting (j_L) and kinetic (j_K) components, and is expressed by the relation: $B = 0.2nFD_0^{2/3}C_0\nu^{-1/6}$ j, in which: n denotes the number of electrons transferred per oxygen molecule, F is the Faraday constant (96,485 C mol^{-1}), D_0 is the diffusion coefficient of oxygen (2.0×10^{-5} cm^2 s^{-1} in 0.1 M $HClO_4$), C_0 refers to the bulk concentration of oxygen (1.5×10^{-3} mol L^{-1} in 0.1 M $HClO_4$), ν indicates the kinematic viscosity, taken as 0.01 cm^2s^{-1} for 0.1 M $HClO_4$.

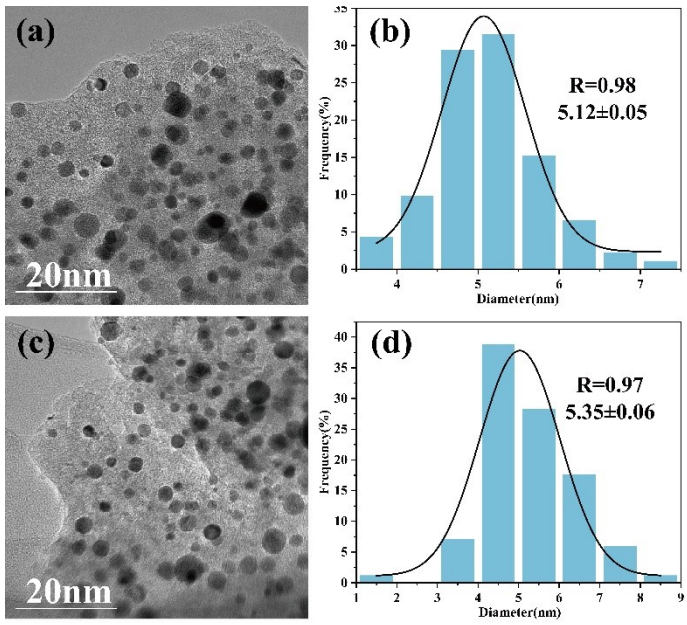

Figure S1. The TEM images and the corresponding particle size distribution histograms of the (a, b) PtFe/NC and (c, d) PtNi/NC catalysts.

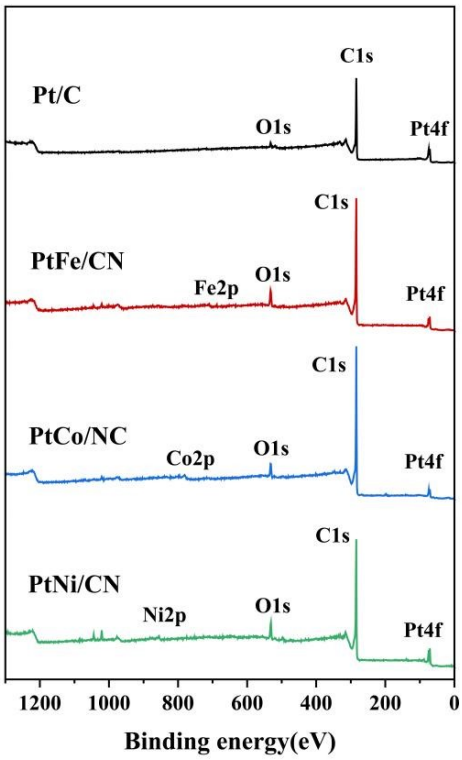

Figure S2. The XPS survey spectrum of commercial Pt/C, PtFe/NC, PtCo/NC, and PtNi/NC catalysts. It can be detected that there are C, N, Pt elements, Co in PtCo/NC, Fe in PtFe/NC, and Ni in PtNi/NC.

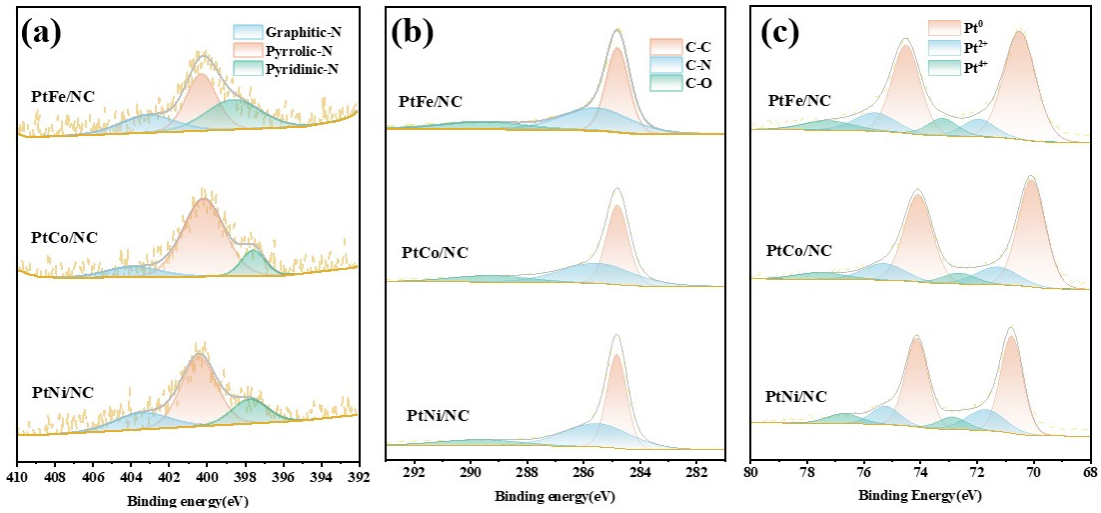

Figure S3. (a-c) XPS spectroscopy of N 1s (a), C 1s (b), and Pt 4f (c) for PtCo/NC, PtFe/NC, and PtNi/NC are presented.

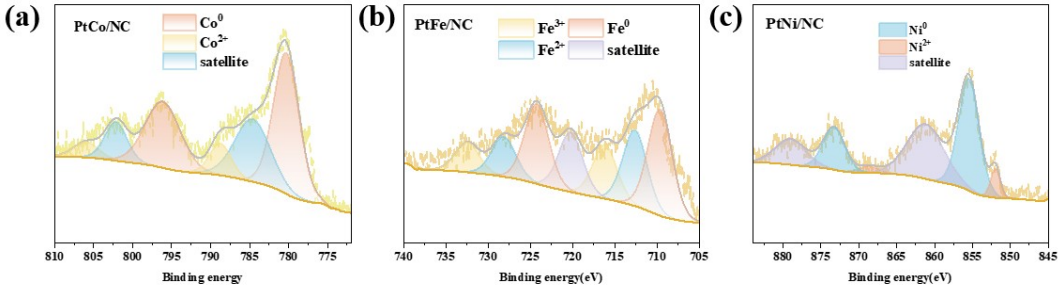

Figure S4. XPS spectra of PtFe/NC Fe2p, PtCo/NC Co2p, PtNi/NC Ni2p. The high-resolution Fe 2p, Ni 2p and Co 2p spectrum for the PtM/NC catalyst is deconvoluted into two pairs of doublets, assigned to Fe species (Fe and Fe^{2+}), Ni species (Ni and Ni^{2+}) and Co species (Co and Co^{2+})

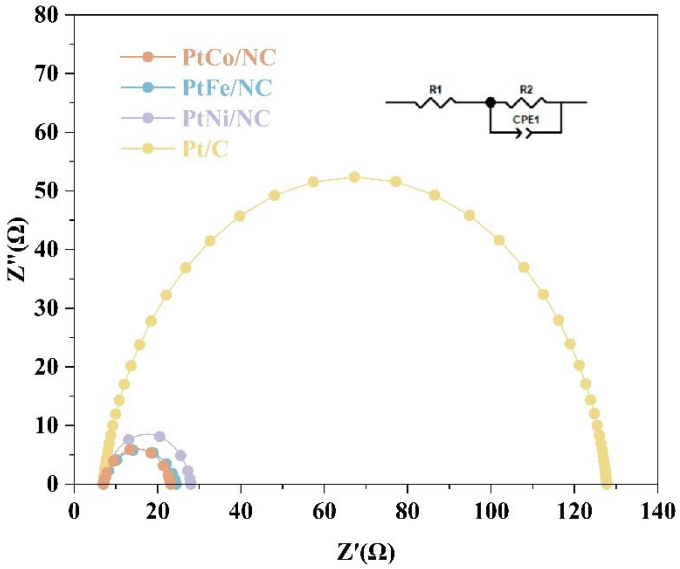

Figure S5. The EIS diagrams of PtM/NC and commercial Pt/C.

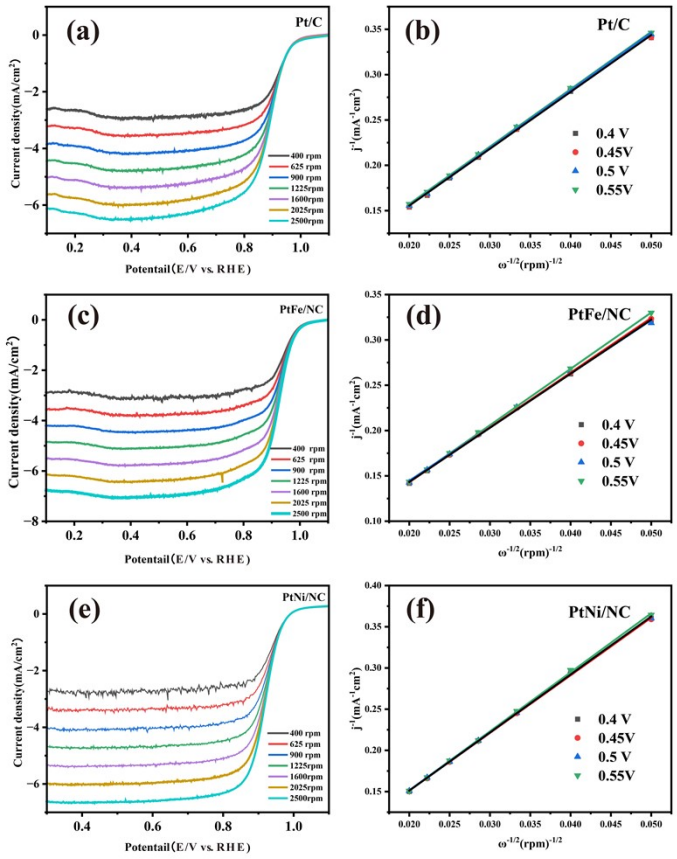

Figure S6. ORR polarization curves of Pt/C, PtFe/NC and PtNi/NCat various rotation rates and Koutecky-Levich plots at various electrode potentials (inset).

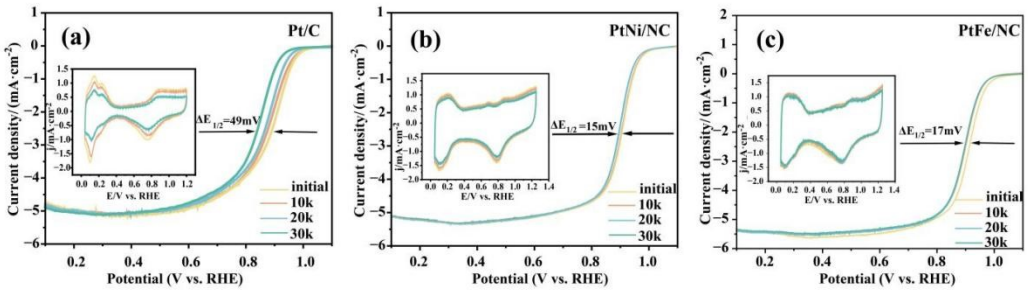

Figure S7. ORR polarization curves of the Pt/C, PtFe/NC and PtNi/NC catalysts before and after 30,000 sweeping cycles by applying15,000CV, 30,000 CV cycles of potential sweeps between 0.6 and 1.1 vs RHE in O_2-saturated 0.1 M $HClO_4$ at a scan rate of 50mV·s^{-1}

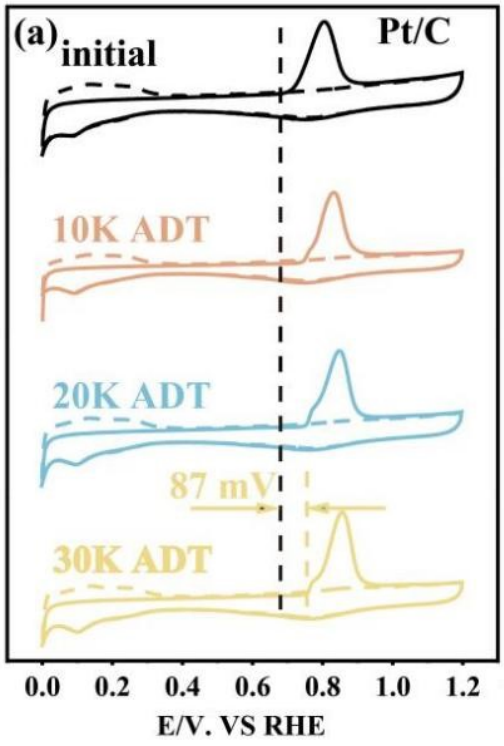

Figure S8. CO stripping voltammograms of the Pt/C sample after ADT.

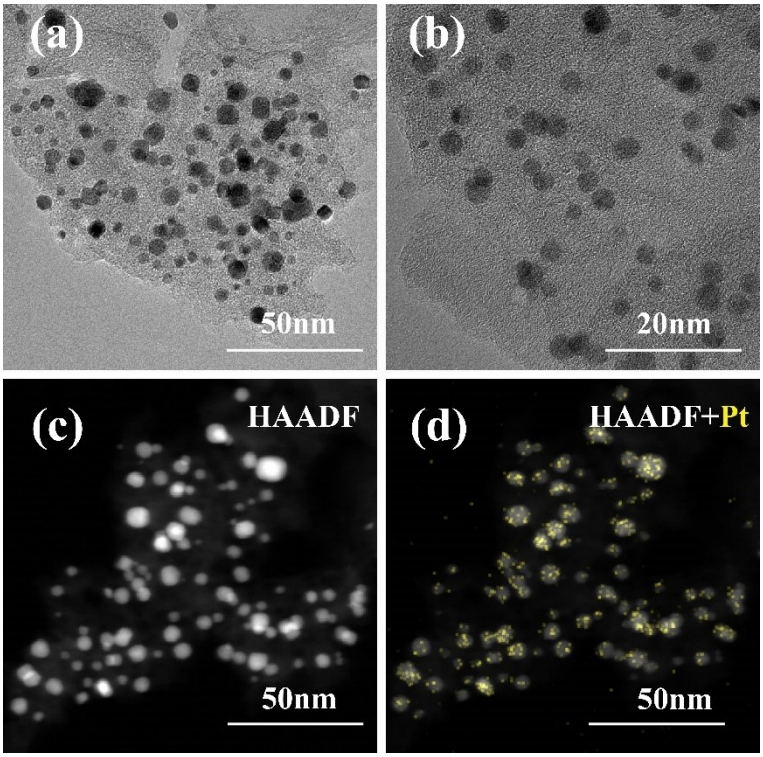

Figure S9. The TEM and elemental mapping of PtCo/NC after ADT.

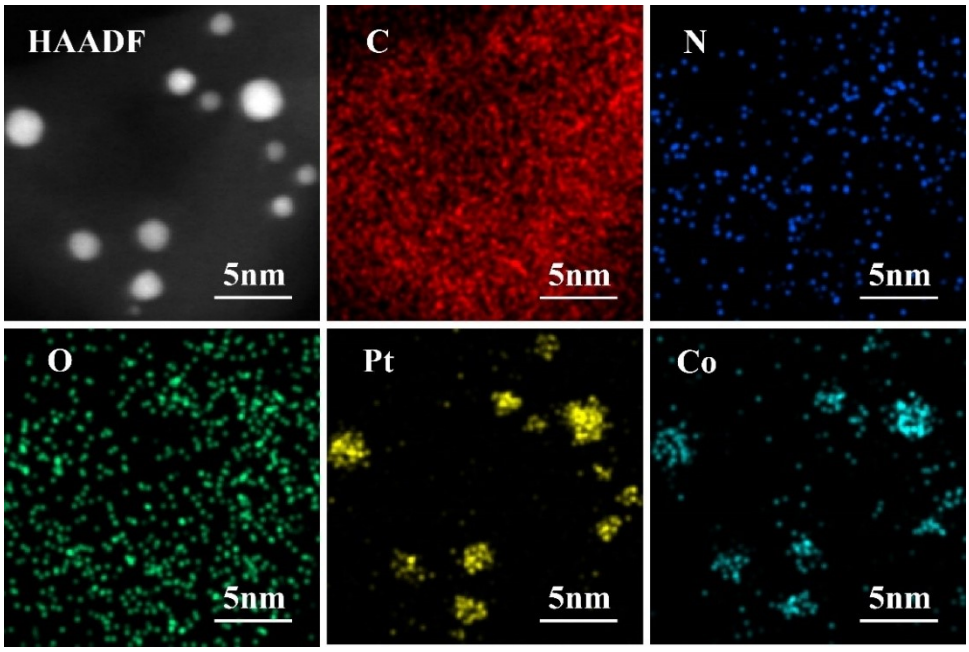

Figure S10. The elemental mapping of PtCo/NC after ADT.

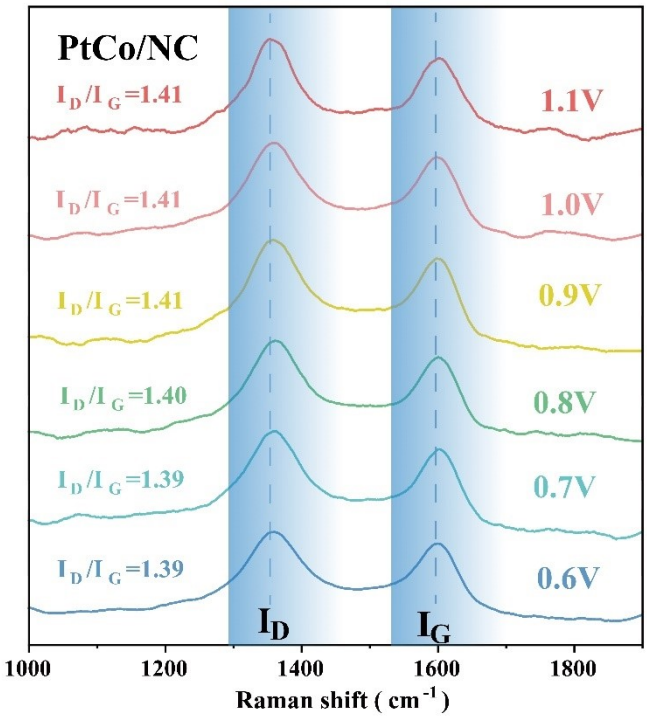

Figure S11. In situ Raman spectra of the PtCo/NC catalyst recorded under different applied potentials (0.6-1.1 V). Two characteristic bands, centered at ~1350 cm^{-1} (D band) and 1590 cm^{-1} (G band), are clearly observed for all voltages.

Note: As the potential increases, both peaks remain in nearly identical positions with no evident broadening or distortion, indicating that the carbon framework preserves its structural integrity during potential variation. The intensity ratio I_D/I_G exhibits only a slight change, increasing marginally from 1.39 at 0.6-0.7 V to 1.41 at 0.9-1.1 V. This negligible variation suggests that the applied voltage does not introduce additional defects into the nitrogen-doped carbon matrix, and the NC carrier maintains a stable degree of disorder in the tested potential window.

Table S1. Lattice Strain of PtCo/NC, PtFe/NC, PtNi/NC and Pt/C

Sample	I_{110}/I_{111}	I_{001}/I_{111}	Lattice Strain (%)
PtCo/NC	0. 267	0. 278	2. 74
PtFe/NC	0. 233	0. 256	2. 56
PtNi/NC	0. 264	0. 265	2. 47

Table S2. The elemental loadings of PtCo/NC, PtFe/NC and PtNi/NC catalysts were determined by using ICP.

Catalyst	ICP (Before Stability test) Loading by weight % relative to the whole sample		ICP (After Stability test) Loading by weight % relative to the whole sample	
	Pt	M(Co、Fe、Ni）	Pt	M(Co、Fe、Ni）
PtCo/NC	18.4	18.6	18.1	18.3
PtFe/NC	20.6	19.4	19.1	18.2
PtNi/NC	19.7	19.1	18.3	18.2

Table S3. Analysis of XPS elements in different catalysts

Sample	C 1s(%)	N 1s(%)	O 1s(%)	Pt 4f(%)	Fe 2p(%)	Co 2p(%)	Ni 2p(%)
PtFe/NC	90.74	1.03	7.34	0.53	0.36	N.A	N.A
PtCo/NC	92.77	0.36	5.40	0.35	N.A	0.87	N.A
PtNi/NC	90.56	0.99	6.99	0.73	N.A	N.A	0.74
Pt/C	95.54	0.33	3.10	1.04	N.A	N.A	N.A

Table S4. The percentages of Fe^{3+}, Fe^{2+}, Fe^{0} and satellite in the Fe2p spectrum of PtFe/NC. The percentages of Co^{3+}, Co^{0} and satellite in the Co 2p spectrum of PtCo/NC. The percentages of Ni^{2+}, Ni^{0} and satellite in the Ni 2p spectrum of PtNi/NC.

Sample	M^{3+}		M^{2+}		M^{0}		satellite	
	Binding energy(eV)	Relative Ratio(%)	Binding energy(eV)	Relative Ratio(%)	Binding energy(eV)	Relative Ratio(%)	Binding energy(eV)	Relative Ratio(%)
PtFe/NC	716.16 732.43	53.02	712.59 728.11	18.11	709.64 724.22	21.20	720.20	7.67
PtCo/NC	780.29 796.13	56.74	783.17 802.11	14.27	N.A. N.A.	N.A.	786.54 805.54	28.99
PtNi/NC	N.A. N.A.	N.A.	855.47 873.24	51.42	851.97 868.62	6.34	861.17 879.65	42.24

Table S5. Relative ratios and binding energy of graphite N, pyridine N, and pyrrole N in the N1s spectrum.

Sample	Graphitic-N		Pyrrolic-N		Pyridinic-N	
	Binding energy(eV)	Relative Ratio(%)	Binding energy(eV)	Relative Ratio(%)	Binding energy(eV)	Relative Ratio(%)
PtCo/NC	403.89	1.91	400.18	80.52	397.57	17.56
PtFe/NC	403.11	9.74	400.30	42.01	398.63	48.25
PtNi/NC	403.41	0.24	400.13	85.70	397.76	14.06

Table S6. The Pt 4f XPS spectra binding energy and the relative ratio of Pt^0, Pt^{2+}, and Pt^{4+} of PtCo/NC, PtFe/NC and PtNi/NC.

Sample	Pt^{4+}		Pt^{2+}		Pt^0	
	Binding energy(eV)	Relative Ratio(%)	Binding energy(eV)	Relative Ratio(%)	Binding energy(eV)	Relative Ratio(%)
PtCo/NC	73.24 77.48	13.05	71.53 75.51	8.86	71.05 74.38	78.09
PtFe/NC	72.92 77.69	12.25	71.07 75.02	7.16	70.73 74.08	80.59
PtNi/NC	73.05 76.65	6.19	71.19 75.23	19.97	70.81 74.13	73.84

Table S7. Half-wave potential, mass activity, specific activity at 0.9V and ICP loading by weight of PtCo/NC, PtFe/NC, PtNi/NC and commercial Pt/C.

Catalyst	Halfwave potential(V)	Mass activity@0. 9V(A/mg_{pt})	Specific activity@0. 9V (mA/cm^2)	Pt loading of catalyst (ICP)
Pt/C	0.887	0.165	0.23	20.3
PtCo/NC	0.927	1.262	2.67	18.4
PtFe/NC	0.926	1.134	1.97	20.6
PtNi/NC	0.921	0.963	2.36	19.1

Table S8. Comparison of MA and SA data before and after ADT of PtCo/NC, PtFe/NC, PtNi/NC and commercial Pt/C.

Catalyst	MA (before ADT) (A/mg_{pt})	SA (before ADT) (mA/cm^2)	MA (after ADT) (A/mg_{pt})	SA (after ADT) (mA/cm^2)
Pt/C	0.165	0.23	0.080	0.119
PtCo/NC	1.262	2.67	1.073	2.31
PtFe/NC	1.134	1.97	0.958	1.674
PtNi/NC	0.963	2.36	0.814	1.925

Table S9. Recent ORR performance comparison of various catalysts.

Sample	MA (A/mg_{pt})	SA (mA/cm^2)	Electrolytes	References
O-PtCo@CoNC	1.21	1.12	0.1 M HClO4	[1]
PtCo-$meso_{4.5}$	0.479	0.416	0.1 M HClO4	[2]
L10 -PtCo/MS-CoNC	0.54	0.91	0.1 M HClO4	[3]
PtCo/C-NBA	0.437	0.751	0.1 M HClO4	[4]
PtCo/NSP-C	1.18	3.17	0.1 M HClO4	[5]
Ni-HIF Pt	0.53	1.17	0.1 M HClO4	[6]
Pt_3Fe/SWCNT	0.697	0.952	0.1 M HClO4	[7]
PtFe	1.134	1.97	0.1 M HClO4	This work
PtCo	1.262	2.67	0.1 M HClO4	This work
PtNi	0.963	2.36	0.1 M HClO4	This work

Reference

[1] H. Chen, Y. Tang, X. Chen, X. Mao, M. Zhang, W. Huang, F. Xie, J. Chen, N. Wang, Y. Jin, H. Meng, Simple solid-state synthesis of platinum alloys on multi-element co-doped carbon supports for efficient and durable oxygen reduction reaction, Int. J. Hydrogen Energy 99 (2025) 761-768.

[2] J. He, C. Chen, H. Yu, Y. Zhao, M. Xu, T. Xiong, Q. Lu, Z. Yu, K. Tai, J. Tan, C. Liu, Epitaxial growth of highly atomically ordered Pt-Fe nanoparticles from carbon nanotube bundles as durable oxygen reduction electrocatalysts, J. Mater. Sci. Technol. 212 (2025) 139-147.

[3] G. Luo, M. Song, L. An, X. Huang, Q. Zhang, C. Zhang, T. Shen, S. Wang, D. Wang, Synergistically enhanced ORR and HER performance on Co-N-C coupled in-situ generated PtCo intermetallic, J. Energy Chem. 100 (2025) 721-729.

[4] Y. Nie, Q. Li, C. Jia, X. Zheng, Z. Shi, S. Wang, Q. Meyer, X.-H. Li, C. Zhao, Mesoporous Co-N-C Supported L10-PtCo Alloy Enables Fast Mass Transport for Proton Exchange Membrane Fuel Cells, Small (2025) e05914-e05914.

[5] K. Song, F. Kong, R. Shen, X. Yu, H. Tian, Q. Guo, G. Zhang, W. Sun, X. Cui, Intensified gas diffusion in ordered mesoporous PtCo alloys for enhanced oxygen reduction electrocatalysis, J. Mater. Chem. A 13 (2025) 6407-6416.

[6] F. Tan, H. Cui, D. He, Y. Hao, W. Ma, Y. Zhao, Y. Liu, C. Wang, F. Liu, J. Liu, K. Jiang, Optimizing alcohol solvents for the synthesis of PtCo alloy catalysts for high-efficient oxygen reduction reaction, J. Alloys Compd. 1017 (2025) 179072.

[7] M. Wang, N. Jiang, B. Huang, H. Jin, L. Guan, S-doped carbon anchoring PtCo intermetallic nanoparticles for efficient proton exchange membrane fuel cells based on molecularly engineered design, J. Power Sources 613 (2024) 234859.